# Molecular Dynamics Simulations of Self-Diffusivities, Corrected Diffusivities, and Transport Diffusivities of Light Gases in Four Silica Zeolites To Assess Influences of Pore Shape and Connectivity

**Anastasios I. Skoulidas and David S. Sholl***

*Department of Chemical Engineering, Carnegie Mellon University, Pittsburgh, Pennsylvania 15213*

*Received: May 23, 2003; In Final Form: August 7, 2003*

We have used equilibrium molecular dynamics (EMD) to study the influences of pore shape and connectivity on single component diffusion of several gases in silica zeolites using atomically detailed models of these materials. Results are presented for $CH_4$, $CF_4$, $SF_6$, Ar, and Ne in silicalite, $CH_4$, Ar, and Ne in ITQ-3, $CH_4$, $CF_4$, Ar, and $SF_6$ in ITQ-7, and $CH_4$, $CF_4$, Ar, and $H_2$ in ZSM-12 at room temperature. This set of four silica zeolites includes one, two, and three-dimensional pore topologies and pore volumes of several different shapes. EMD can be used to simultaneously determine the self-diffusivities and corrected diffusivities as a function of pore loading, and this has been done for every example. In combination with adsorption isotherms computed using grand canonical Monte Carlo, EMD results can also determine the transport diffusivity as a function of pore loading. The resulting transport diffusivities are reported for every example. The broad data set presented here is useful for considering the variety of diffusion behaviors that can occur for small molecules adsorbed in zeolite pores.

## I. Introduction

Molecular diffusion plays a key role in many applications of zeolites to practical processes. Intracrystalline diffusion can be a rate-limiting step in the use of zeolites as catalysts.[1−3] Diffusion rates are one crucial factor in determining the flux and selectivity of zeolitic membranes.[4,5] Because molecules are tightly confined inside the pores of zeolites, their diffusion rates are strongly affected by the relative size and shape of the molecules and pores, the local chemical environment defined by the presence or absence of framework substitutions and cations, and the connectivity of the zeolite pores.[1−3]

The diffusion rate of an adsorbed species with concentration $c$ inside a zeolite is described by several distinct quantities.[1,2,6] The self-diffusivity, $D_s(c)$, measures the displacement of a tagged molecule as it diffuses at equilibrium. The self-diffusivity is conveniently defined using the Einstein expression

$$D_s(c) = \lim_{t\to\infty} \frac{1}{6t}\langle|\vec{r}(t) - \vec{r}(0)|^2\rangle \tag{1}$$

Here, $\vec{r}(t)$ is the position of the tagged particle at time $t$. This expression has been written in terms suitable for an isotropic three-dimensional medium but is easily generalized to anisotropic materials. Macroscopic diffusion of a single adsorbed species in a zeolite can be characterized using the transport diffusivity, $D_t(c)$, which is defined as the proportionality constant relating a macroscopic flux, $\vec{J}$, to a macroscopic concentration gradient:

$$\vec{J} = -D_t(c)\nabla c \tag{2}$$

Again, this expression is suitable for an isotropic medium but can be easily generalized to anisotropic materials. Recognizing that the chemical potential is a more appropriate driving force for diffusion in microporous materials than concentration,[1,2,6] the transport diffusivity is often rewritten as

$$D_t(c) = D_0(c)\left(\frac{\partial \ln f}{\partial \ln c}\right)_T \tag{3}$$

Here, $f$ is the fugacity of the bulk phase that is at equilibrium with the adsorbed phase when the latter has concentration $c$, and $D_0(c)$ is called the corrected diffusivity.[6,7] The term involving the logarithmic derivative of the fugacity is referred to as the thermodynamic correction factor and can be evaluated provided the equilibrium adsorption isotherm for the material being studied is known. For systems in which only a single chemical species is adsorbed, the corrected diffusivity is identical to the Maxwell−Stefan (MS) diffusivity in the widely used MS formulation of mass transport.[8−10]

The self-diffusivity, transport diffusivity, and corrected diffusivity (denoted $D_s(c)$, $D_t(c)$, and $D_0(c)$, respectively, throughout this paper) have been written in a form that emphasizes the fact that they are concentration dependent and, in general, not equal to each other.[1,2,6] The three diffusivities do become equal in the limit of zero adsorbate concentration,[1,2,6] and we denote this limiting diffusivity by $D_0$:

$$D_s(c{=}0) = D_t(c{=}0) = D(0)(c{=}0) = D(0) \tag{4}$$

Long-standing controversies exist regarding the experimental measurement of molecular diffusivities in zeolites with experimental methods that measure differing aspects of diffusion.[1,2,11] Making comparisons between the different diffusivities defined above, particularly the self-diffusivity and transport diffusivity, requires some means of understanding the concentration dependence of each quantity. Although there are several approximations used for this type of analysis, for example, the so-called Darken approximation that takes the corrected diffu-

* Corresponding author. Fax: 412-268-7139. E-mail: sholl@andrew.cmu.edu.

10.1021/jp0354301 CCC: $25.00 
Published on Web 11/01/2003

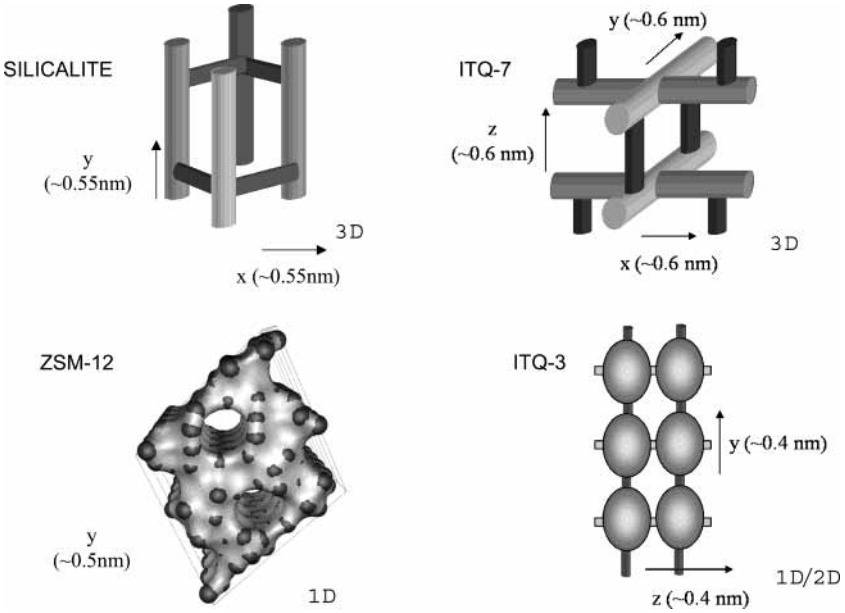


**Figure 1.** Schematic illustrations of the pore topology of silicalite, ITQ-7, ZSM-12, and ITQ-3. The pore diameters listed for each channel direction give the approximate diameter of the narrowest portion of the pore.

sivity to be concentration independent,[6,12] little is known about the accuracy of these approximations. Atomically detailed simulations have an important role to play in remedying this situation. We have recently shown that equilibrium molecular dynamics (EMD) methods can be used to simultaneously measure the self-diffusivities and corrected diffusivities for a broad range of simple molecules adsorbed as single components in silicalite, a prototypical noncationic zeolite.[6,13] By using grand canonical Monte Carlo (GCMC) to determine the adsorption isotherm for the species of interest, the transport diffusivity for these species can also be unambiguously determined using eq 3. That is, methods now exist that allow $D_s(c)$, $D_t(c)$, and $D_0(c)$ to be calculated in a fully self-consistent manner once the crystal structure of the zeolite of interest and the interatomic potentials defining the interactions of the guest molecules with the zeolite are specified. Experimental methods that can simultaneously assess self-diffusivities and transport diffusivities are available in some cases,[11,14] but the number of examples that have been studied in this way to date is very limited.

It is useful to note that the atomically detailed methods mentioned above are not restricted to single-component adsorption. Extending earlier work by Sanborn and Snurr,[15,16] we have recently used EMD methods to quantify the binary-component generalizations of the self-diffusivities and transport diffusivities for $CH_4/CF_4$ mixtures in silicalite. The resulting diffusivities allowed the first direct comparison between predictions from a fully atomistic model and experimental measurements of binary permeance through a polycrystalline zeolite membrane.[17] They also offer a useful test case for examining approximate methods for predicting mixture diffusivities from single-component data.[10]

In this paper, we present concentration dependent self-diffusivities, corrected diffusivities, and transport diffusivities determined using EMD for a number of light gas molecules adsorbed in four silica zeolites with different pore shapes and connectivities. All results are for adsorption at room temperature. This is the first time that simultaneous calculations of self-diffusivities and transport diffusivities have been made for zeolites other than silicalite. The four zeolites examined here are ZSM-12,[18] ITQ-3,[19] ITQ-7,[20] and silicalite.[21] The pore topologies of these four materials are shown schematically in Figure 1. ZSM-12, silicalite, and ITQ-7 each have approximately cylindrical pores, whereas ITQ-3 has cages connected by small pores. Silicalite and ITQ-7 both have a three-dimensional pore topology. ZSM-12 has a one-dimensional pore topology. The topology of ITQ-3 is two-dimensional for small molecules but one-dimensional for larger molecules, as will be described in more detail below. We note that it would be more formally correct to refer to the all silica structures of silicalite, ITQ-3, ITQ-7, and ZSM-12 as MFI-type silica, ITE-type silica, ISV-type silica, and MTW-type silica, but we will refer below to each material in the former manner for convenience.

The paper is organized as follows. Section II provides a description of our interatomic potentials and simulation methods, together with some comments on the pore structure of the four zeolites. The adsorption isotherms of the species of interest are described in section III. The self-diffusivities, corrected diffusivities, and transport diffusivities for each adsorbed species are described in sections IV−VI, respectively. The paper concludes in section VII with a discussion of the implications of our results.

## II. Methods

Molecular dynamics and Monte Carlo simulations of light gases adsorbed in silica zeolites were performed using methods very similar to those of our previous work on gas adsorption in silicalite.[6,13] Interactions between adsorbed molecules and the zeolites were defined by a pairwise sum of Lennard-Jones interactions between the spherical adsorbed molecules and the O atoms in the zeolite framework. The adsorbate-framework potentials ($\epsilon_{AZ}$ and $\sigma_{AZ}$) and adsorbate−adsorbate potentials ($\epsilon_{AA}$ and $\sigma_{AA}$) were taken to be the same as in our earlier work on silicalite for $CH_4$, $CF_4$, Ne, Ar, and $SF_6$[6,13] and our earlier work on ZSM-12 for $H_2$.[22] These parameters are summarized in Table 1. In all calculations, each zeolite was assumed to be rigid in the crystallographic structure determined experimentally. Some details of these structures are summarized in Table 2, and the pore connectivities of each material are illustrated in Figure 1.

Self-diffusivities and corrected diffusivities were computed simultaneously from trajectories obtained from equilibrium MD simulations using the Einstein relations available for these two

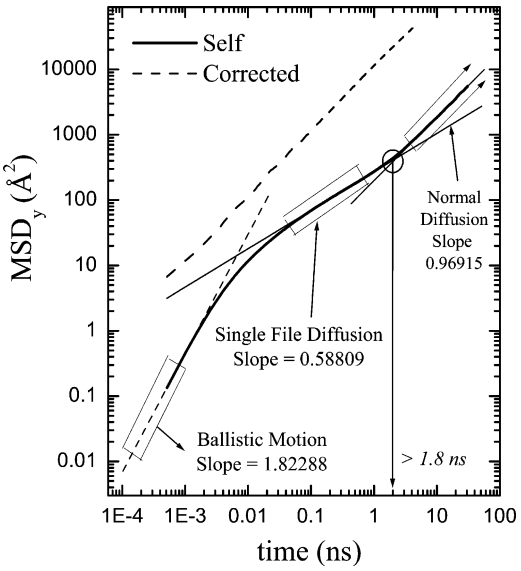


**Figure 2.** Observed MSD for $CF_4$ in ZSM-12 at 298 K at a loading of one molecule per unit cell. The solid curve shows data from self-diffusion, with the fitted curves indicating the transitions from ballistic motion to single-file diffusion to normal diffusion. The upper dashed curve shows data from the corrected diffusivity from the same set of simulations.

**TABLE 1: Interatomic Potential Parameters for the Adsorbates Considered in This Work**

| Adsorbate | Ref. | $\epsilon_{AA}$ (K) | $\sigma_{AA}$ (Å) | $\epsilon_{AZ}$ (K) | $\sigma_{AZ}$ (Å) |
|---|---|---|---|---|---|
| $CH_4$ | Goodbody et al.[45] | 147.9 | 3.73 | 133.3 | 3.214 |
| $CF_4$ | Heuchel et al.[46] | 134.0 | 4.66 | 109.6 | 3.73 |
| $H_2$ | Skoulidas et al.[22] | 34.02 | 2.96 | 51.233 | 2.62 |
| Ne | Skoulidas et al.[13] | 35.7 | 2.789 | 56.87 | 2.798 |
| Ar | Clark et al.[47] | 124.07 | 3.42 | 95.61 | 3.17 |
| $SF_6$ | Clark et al.[47] | 222.1 | 5.13 | 147.21 | 3.97 |

diffusivities.[2,6,7,13] Computing corrected diffusivities from EMD simulations requires averaging over multiple independent simulations.[6,7,13] In each case, a minimum of 20 independent simulations were used for this purpose.

We have discussed the requirements for equilibrating and converging EMD calculations of light gases in silicalite elsewhere,[13] and similar procedures were used here for the other silica zeolites. The smallest simulation volumes used in our calculations were $3 \times 3 \times 2$ unit cells for ITQ-7, $2 \times 6 \times 2$ unit cells for ITQ-3, and $2 \times 10 \times 2$ unit cells for ZSM-12. At the lowest adsorbate densities considered, the simulation volumes were increased in size to include at least 50 adsorbed molecules in each simulation.

The only example that requires a special comment related to convergence is ZSM-12. The one-dimensional channels of ZSM-12 open the possibility that for large adsorbates, diffusion may occur following single-file diffusion rather than normal diffusion.[23−28] In this case, eq 1 is not valid and the mean-square displacement of a tagged particle is given by

$$\lim_{t\to\infty} \langle |\vec{r}(t) - \vec{r}(0)|^2 \rangle = 2F\sqrt{t} \qquad (5)$$

where $F$ is referred to as the single-file mobility. This expression is valid if adsorbates are prohibited from passing one another in a one-dimensional pore. A more general situation occurs when it is extremely difficult for adsorbates to pass one another in a pore, but passage can be observed on sufficiently long time scales.[26,27,29,30] In this case, the scaling of eq 5 is expected to be valid for time scales that are shorter than the mean time for particles to pass one another, but eq 1 will be recovered on sufficiently long time scales. It is this situation that applies to the adsorbates we have simulated in ZSM-12. This point is illustrated in Figure 2 for $CF_4$, the largest adsorbate we have considered in ZSM-12. Figure 2 shows the observed MSD for tagged $CF_4$ molecules in ZSM-12 at a pore loading of one molecule per unit cell. At extremely short times, the motion of each adsorbate is ballistic, so $\langle |\vec{r}(t) - \vec{r}(0)|^2 \rangle \sim t^2$. On time scales of multiple nanoseconds, the observed MSD is linear in time, indicating that normal diffusion occurs on these time scales. There is an intermediate regime in the time where the slope of the MSD on the log−log plot of Figure 2 is approximately 0.5. $CF_4$ self-diffusion in this regime occurs in a single-file manner. The general behavior of the crossover time between single-file and normal diffusion in systems where passing of adsorbates is rare has been carefully examined by Hahn and Kärger.[30] For the smaller adsorbates we have simulated in ZSM-12, this single-file regime is much less pronounced. Below, all of the self-diffusivities for gases in ZSM-12 have been determined from the MSD after excluding the transient regime of ballistic and single-file diffusion. Determining corrected diffusivities from EMD trajectories involves examining the MSD associated with the motion of the center of mass of the adsorbates in each simulation.[6,7,13] Figure 2 also shows this MSD. This quantity, which is a collective property of the entire system of diffusing adsorbates, is linear in time over the whole range of data shown in Figure 2. This observation emphasizes previous demonstrations that the corrected and transport diffusivities are well-defined quantities even in physical systems that exhibit single-file diffusion of tagged particles.[31]

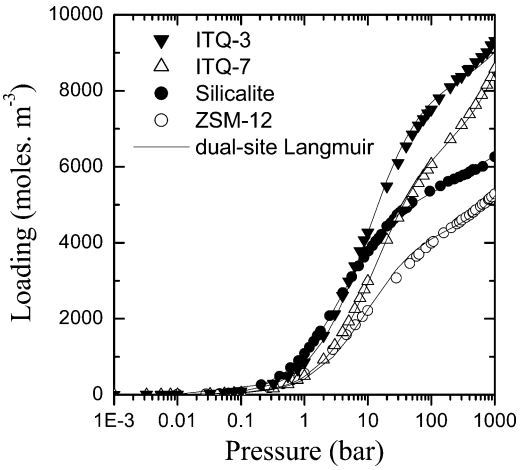


**Figure 3.** Adsorption isotherms determined using GCMC for $CH_4$ in silicalite, ITQ-3, ITQ-7, and ZSM-12 at 298 K. The uncertainty in each data point is smaller than the symbol size.

## III. Adsorption Isotherms

The adsorption isotherms for each adsorbed species at 298 K were computed using standard GCMC methods.[32] The chemical potential of each gas-phase species was related to the gas-phase pressure through the virial equation of state using a fourth order virial expansion for $CH_4$ and $CF_4$ and a third-order expansion for the rest of the species studied. The virial coefficients for $CH_4$ and $CF_4$ were taken from Doulsin et al.[33] The rest of the coefficients were taken from Dymond et al.[34] An example of our results is shown in Figure 3, which shows the calculated isotherms for $CH_4$ in all four of the silica zeolites we have studied. The minor differences in adsorption capacity between the four zeolites can be correlated with the different pore volumes available in these materials.[35]

**TABLE 2: Structural Information for the Silica Zeolites Considered in This Work**

| Zeolite | Ref. | Topology | Unit Cell | Channels |
|---|---|---|---|---|
| Silicalite | Olson et al.[21] | 3D | a = 20.07, *b* = 19.92, *c* = 13.42 Å<br>Orthorhombic (P*nma*) | x − 5.1 × 5.5 Å<br>y − 5.3 × 5.6 Å |
| ITQ-7 | Villaescusa et al.[20] | 3D | a = 12.853, *b* = 25.214 Å<br>Tetragonal (*P*4$_2$/*mmc*) | x/y − 6.1 × 6.5 Å<br>z − 5.9 × 6.6 Å |
| ITQ-3 | Camblor et al.[19] | 1D/2D | a = 20.622, *b* = 9.724, *c* = 19.623 Å<br>Orthorhombic (C*mcm*) | y − 3.8 × 4.3 Å<br>z − 2.7 × 5.8 Å |
| ZSM-12 | Fyfe et al.[18] | 1D | a = 24.863, *b* = 5.012, *c* = 24.328 Å<br>$\alpha = 90$, $\beta = 107.72$, $\gamma = 90°$<br>Monoclinic, (C12/*c*1) | y − 5.6 × 6.0 Å |

**TABLE 3: Dual-site Langmuir Isotherm Parameters for the Light Gases Considered in Each Silica Zeolite**

| Zeolite | Species | $c_1$ | $c_2$ | $c_3$ | $c_4$ | $c_{sat}$ |
|---|---|---|---|---|---|---|
| Silicalite | Ar | 17.63 | 26.78 | 9.32 | 1177 | 27 |
| | Ne | 34.2 | 423.254 | 0 | 0 | 34.2 |
| | $CH_4$ | 17.1 | 4 | 5.5 | 670 | 22.6 |
| | $CF_4$ | 11.9 | 0.44 | 4.2 | 173 | 16 |
| | $SF_6$ | 11 | 0.00284 | 1 | 1.43 | 12 |
| ITQ-7 | Ar | 38.25 | 4097 | 17.81 | 52.36 | 56 |
| | $CH_4$ | 36.68 | 6769 | 16.82 | 13.07 | 53.5 |
| | $CF_4$ | 4.12 | 964.8 | 9.94 | 1.676 | 14 |
| | $SF_6$ | 8.646 | $9.87\ 10^{-3}$ | 1.164 | 6.207 | 9.81 |
| ITQ-3 | $CH_4$ | 36.5 | 18928 | 19.756 | 9.6 | 56.3 |
| | Ar | 25.4 | 4691 | 18.62 | 44.5 | 44 |
| | Ne | 92.53 | 17010 | 36.52 | 635.2 | 129 |
| ZSM-12 | $CH_4$ | 7.62 | 9.63 | 31.73 | 19770 | 39.4 |
| | $H_2$ | 7.92 | 287.5 | 30 | 10924 | 37.9 |
| | $CF_4$ | 3.6 | 0.5285 | 0.76 | 165.1 | 4.4 |
| | Ar | 5.88 | 31.2 | 6.57 | 758.87 | 12.5 |

$c_1$, $c_3$, and $c_{sat}$ have units of molecules/unit cell. $c_2$ and $c_4$ have units of atm.

The adsorption isotherm for each species considered was fitted using the dual-site Langmuir form

$$c = \frac{c_1 P}{c_2 + P} + \frac{c_3 P}{c_4 + P} \tag{6}$$

In Figure 3 the lines represent the isotherms given by eq 6 for each zeolite. The average relative percent difference between the fitted isotherms and the GCMC results is less than 1% for silicalite, 10% for ZSM-12, 2.5% for ITQ-7, and 5% for ITQ-3. At the highest loadings studied the relative percent difference between the fitted isotherms and the GCMC results were less than 1% for all zeolites considered. The parameters determined in these fits are summarized in Table 3. This table also lists the saturation loading for each species implied by these isotherms, $c_{sat}$. We note that this definition of the saturation loading is somewhat different than one we used in our earlier work,[13] but the practice of determining the saturation loading from a fitted isotherm is more practical experimentally than our previous methods. Most of our results below will be presented in terms of the fractional loading of adsorbed species, $\theta = c/c_{sat}$.

## IV. Self-Diffusion

We began our investigation of self-diffusion in the silica zeolites of interest by calculating the infinite dilution diffusivity, $D(0)$, of each light gas species studied at 298 K. The diffusivity in this limit can be calculated with high accuracy by performing EMD simulations of many adsorbed particles with no adsorbate−adsorbate interactions. As noted in eq 4, the self-diffusivities, corrected diffusivities, and transport diffusivities of any adsorbate are equal in the limit of infinite dilution. The values of $D(0)$ for each system are summarized in Table 4. Here and below, we report only the orientationally averaged diffusivity

**TABLE 4: Infinite Dilution Diffusivities, $D(0)$, of the Light Gas Species in Each Silica Zeolite in Units of $10^{-4}$ cm$^2$·s$^{-1}$**

| zeolite | species | $D(0)$ | zeolite | species | $D(0)$ |
|---|---|---|---|---|---|
| ITQ-7 | Ar | 3.19 | silicalite | Ar | 1.32 |
| | $CH_4$ | 4.06 | | Ne | 2.74 |
| | $CF_4$ | 1.43 | | $CH_4$ | 1.45 |
| | $SF_6$ | 0.64 | | $CF_4$ | 0.45 |
| ZSM-12 | $CH_4$ | 6.24 | | $SF_6$ | 0.053 |
| | $H_2$ | 35.0 | ITQ-3 | $CH_4$ | 0.166 |
| | $CF_4$ | 6.36 | | Ar | 0.23 |
| | Ar | 5.49 | | $Ne_y$ | 1.60 |
| | | | | $Ne_z$ | 0.33 |

for adsorbates in silicalite. Diffusion in silicalite is anisotropic, but we have reported extensively on this anisotropy previously.[13] Diffusion in ITQ-7 is slightly anisotropic, and in this case we also only report the orientationally averaged diffusivities. In ITQ-3, $CH_4$ and Ar can diffuse only in the *y* direction because these species cannot penetrate the small pores connecting cages in the *z* direction. Ne, in contrast, can diffuse in both the *y* and *z* directions in ITQ-3. The diffusivities in these two directions are reported separately below. The infinite dilution diffusivities span almost 3 orders of magnitude from the slowest species studied, $SF_6$ in silicalite, to the fastest, $H_2$ in ZSM-12. There is considerable variation in the infinite dilution diffusivity of a single species between the four zeolites studied. For example, the observed diffusivity of $CH_4$ is 38 times faster in ZSM-12 than in ITQ-3, with the values for ITQ-7 and silicalite intermediate between these extremes.

The loading dependence of the self-diffusivity of each adsorbed species studied in silicalite, ITQ-3, ITQ-7, and ZSM-12 is shown in Figures 4−7, respectively. For clarity, the self-diffusivity in each case has been normalized by its infinite dilution value and is shown as a function of the fractional loading of the adsorbate. The absolute values for either the self-diffusivity or the pore loading can be determined with reference to Tables 4 or 3, respectively. We have presented the data for silicalite previously,[13] but show it again here for completeness.

The general trends for the self-diffusivities of each species in silicalite and ITQ-7 (Figures 4 and 6, respectively) are similar: $D_s$ decreases monotonically as the loading is increased. This well-known effect stems from the increased steric hindrance to the motion of a tagged particle due to nearby adsorbates as the loading is increased. The loading dependence of $D_s$ in ITQ-3, shown in Figure 5, is quite different. For $CH_4$ and Ar, the self-diffusivity is an increasing function of loading for dilute loadings. After reaching a maximum value at some intermediate loading, these two self-diffusivities decrease at higher loadings. This qualitative behavior has been observed previously in MD simulations of small molecules diffusing in siliceous ZK4, a zeolite with a similar cage structure to ITQ-3.[36,37] A detailed transition state analysis of this system by Tunca and Ford has shown that the increase in $D_s$ with loading occurs because of collective effects of molecules adsorbed in neighboring cages that act to reduce the energy barrier for molecules to hop

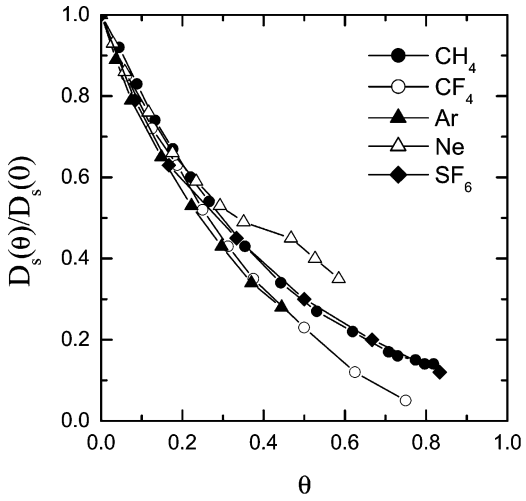


**Figure 4.** $D_s(\theta)/D(0)$ plotted versus $\theta$ for $CH_4$, $CF_4$, $SF_6$, Ar, and Ne in silicalite at 298 K using saturation loadings defined in Table 2.

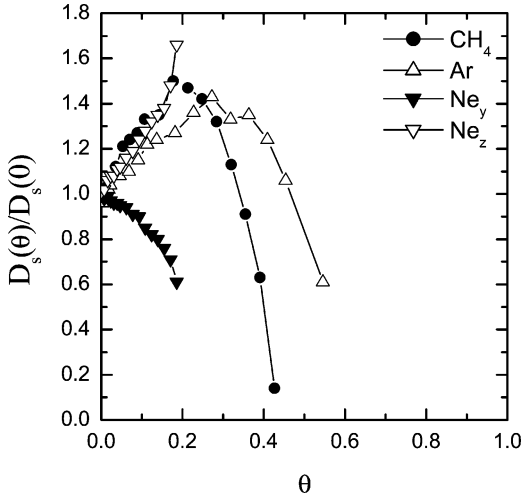


**Figure 5.** Same as Figure 4 but for $CH_4$, Ar, and Ne in ITQ-3.

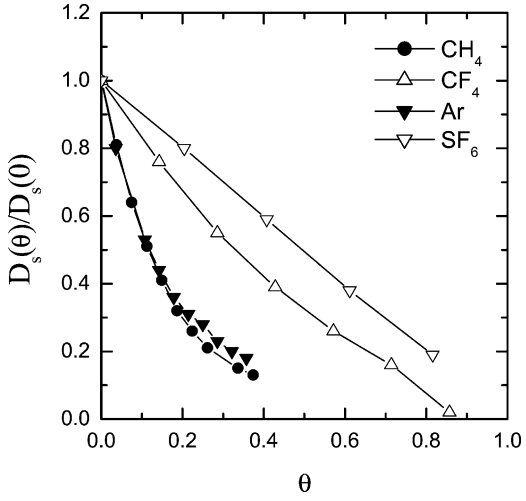


**Figure 6.** Same as Figure 4 but for $CH_4$, $CF_4$, Ar, and $SF_6$ in ITQ-7.

between cages relative to the energy barrier encountered by an isolated molecule.[36,37] At sufficiently high loadings, steric hindrance will offset this energetic change, resulting in a net decrease in the self-diffusivity. Analysis of the potential energy surfaces encountered by isolated molecules of $CH_4$ or Ar in ITQ-3 strongly suggests that the mechanism identified by Tunca and Ford for ZK4 also controls the results shown in Figure 5.

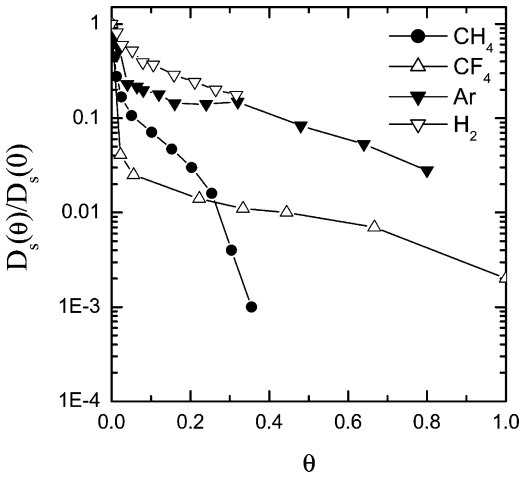


**Figure 7.** Same as Figure 4 but for $CH_4$, $CF_4$, Ar, and $H_2$ in ZSM-12.

The qualitative behavior of Ne in ITQ-3 is somewhat different from that of $CH_4$ or Ar. For diffusion of Ne along the *y* direction, the only direction available to the larger species, the self-diffusivity decreases monotonically as the pore loading is increased. Although we have not analyzed this phenomenon in detail, this observation indicates that the reduction of the cage to cage energy barrier due to adsorbate−adsorbate interactions that occurs for $CH_4$ and Ar does not occur for Ne diffusing in the *y* direction in ITQ-3. The self-diffusivity of Ne in the *z* direction in ITQ-3, in contrast, increases monotonically, at least over the limited range of coverages that we have explored. It seems likely that this occurs because of similar energetic effects to those that govern self-diffusion in the *y* direction for $CH_4$ and Ar.

The loading dependence of the self-diffusivity in ZSM-12 (Figure 7) is quite different from any of the other three materials due to its one-dimensional pores. As discussed in detail above, two molecules of even the largest adsorbate we have examined, $CF_4$, can pass one another in the pores of ZSM-12, so the diffusion of each adsorbate is appropriately described as normal diffusion rather than single-file diffusion. Nevertheless, the difficulty associated with two adsorbates passing one another in this one-dimensional environment greatly enhances the effects of steric hindrance on the observed self-diffusivities relative to those seen in three-dimensional pore structures or in cages. This is seen most dramatically for $CH_4$ and $CF_4$ in ZSM-12, where $D_s$ is reduced by 1 order of magnitude in going from infinite dilution to $\theta = 0.1$ and reduced by another order of magnitude when $\theta$ is further increased to 0.2. As expected, this effect is considerably weaker for smaller molecules, particularly for $H_2$. We have previously observed similarly dramatic changes in self-diffusivities as functions of pore loading for small molecules diffusing in the one-dimensional pores of single-walled carbon nanotubes.[22] One implication of these observations is that it would be very difficult to accurately infer the infinite dilution diffusivity of a large molecule diffusing in a microporous material with one-dimensional pores solely from measurements of the self-diffusivity at finite loading.

It is interesting to compare the loading dependence of the self-diffusivities discussed above with the range of behaviors that has been observed experimentally for molecular diffusion in zeolites. One source that illustrates the diversity of behaviors seen in experiments is Figure 2 of ref 2, which compiles results from a large series of experiments by Kärger and Pfeifer using NaX and NaCaA. Most of the self-diffusivities in our calculations are similar to that of *n*-hexane in NaX in that they decrease monotonically with increasing loading. There are number of

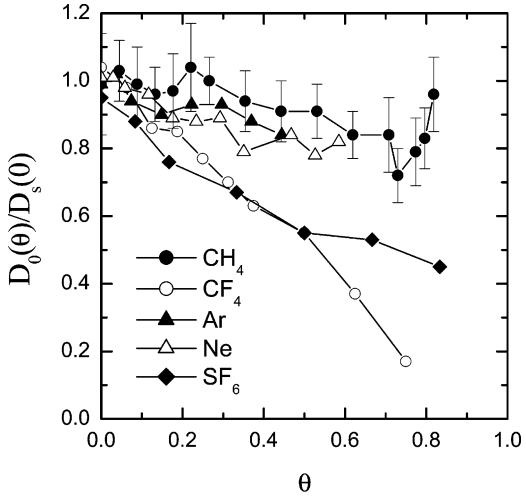


**Figure 8.** $D_0(\theta)/D(0)$ plotted versus $\theta$ for $CH_4$, $CF_4$, $SF_6$, Ar, and Ne in silicalite at 298 K using saturation loadings defined in Table 2.

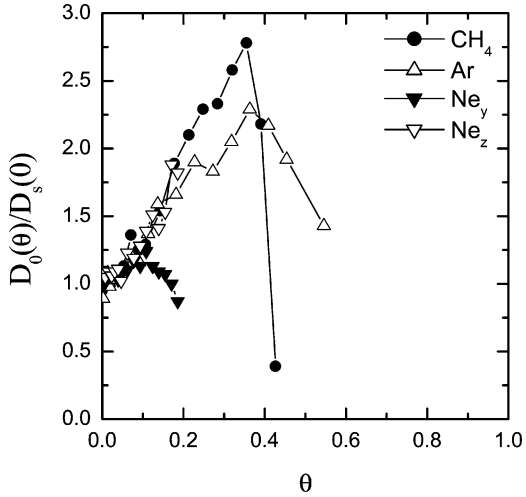


**Figure 9.** Same as Figure 8 but for $CH_4$, Ar, and Ne in ITQ-3.

experimental examples where the self-diffusivity increases with loading, similar to our results for ITQ-3, although there are none in the source cited above that show a distinct maximum. Overall, the range of behaviors that has been observed experimentally is more diverse that we see in our simulations, a fact that stems from the greater diversity of molecular shapes and functionality in the experiments relative to our simulations.

## V. Corrected Diffusion

The loading dependence of the corrected diffusivity, $D_0$, of each adsorbed species studied in silicalite, ITQ-3, ITQ-7, and ZSM-12 is shown in Figures 8−11, respectively. As for the self-diffusivities discussed above, the corrected diffusivity in each case has been normalized by its infinite dilution value and is shown as a function of the fractional loading of the adsorbate. We have presented the data for silicalite previously[13] but show it again here for completeness. It is important to emphasize that the corrected diffusivities are determined directly from our EMD trajectories; no assumptions regarding the functional form of the corrected diffusivity is required to perform this calculation.

The corrected diffusivities for $CH_4$, $CF_4$, $SF_6$, Ar, and Ne in silicalite are presented in Figure 8. These data have been discussed extensively elsewhere,[6,13] so only two comments are needed here. First, the uncertainties indicated on the $CH_4$ data in Figure 8 are representative of the observed uncertainties in all our calculated corrected diffusivities. These uncertainties are intrinsically larger than those associated with calculating self-diffusivities from EMD trajectories. Second, the corrected diffusivities in Figure 8 exhibit a broader range of behaviors than the analogous self-diffusivities (cf. Figure 4). The smaller species have corrected diffusivities that are almost independent of loading, whereas the two largest species, $CF_4$ and $SF_6$, have corrected diffusivities that decrease strongly with loading. These two behaviors have been referred to as the weak confinement and strong confinement scenarios, respectively,[10] and the "strength" of this confinement has been loosely related to the size of the diffusing species. We will see below that this loose identification is not an effective one for the other zeolites we have examined.

The corrected diffusivities for $CH_4$, Ar, and Ne in ITQ-3 are shown in Figure 9. As above, the components of the Ne diffusivity in the *y* and *z* directions are shown separately. The trends observed in this case are quite similar to those seen for the self-diffusivities in ITQ-3 (cf. Figure 5), but very different

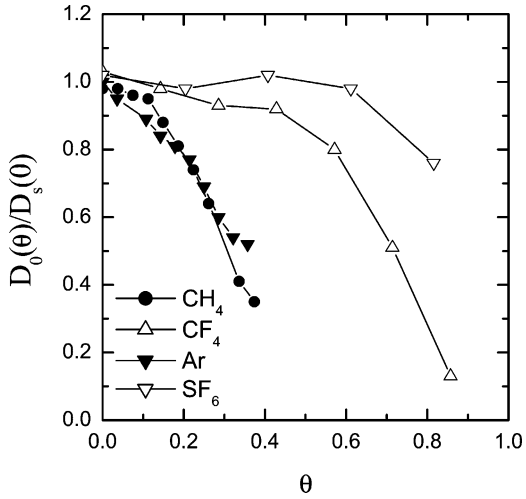


**Figure 10.** Same as Figure 8 but for $CH_4$, $CF_4$, Ar, and $SF_6$ in ITQ-7.

from the corrected diffusivities observed in silicalite. It is interesting to note that the corrected diffusivities of all three species examined increase as the loading is increased, at least for small values of $\theta$.

Figure 10 shows the corrected diffusivities of $CH_4$, $CF_4$, Ar, and $SF_6$ in ITQ-7. At first glance, these results seem similar to those for silicalite; the corrected diffusivity for some species decreases rapidly as pore loading increases, whereas for others $D_0$ is roughly independent of $\theta$, at least for low and moderate loadings. More careful consideration, however, reveals a surprising feature of these results. In silicalite, the smaller adsorbates, including $CH_4$ and Ar, are described by the "weak confinement" scenario in which $D_0$ is approximately constant, whereas the larger species, including $CF_4$ and $SF_6$, are described by the "strong confinement" scenario in which $D_0$ decreases approximately linearly with loading.[10] This situation is reversed in ITQ-7. That is, the smaller species exhibit a corrected diffusivity that decreases strongly with loading, whereas $D_0$ for the two largest species is roughly constant, at least for $\theta \leq 0.6$. This observation confounds the idea that it may be possible to predict the loading dependence of the corrected diffusivity solely from the size of the adsorbate relative to the zeolite pores in which diffusion occurs.

The corrected diffusivity for $CH_4$, $CF_4$, Ar, and $H_2$ in the one-dimensional pores of ZSM-12 is shown in Figure 11. Similar to the results for silicalite and ITQ-7, $CH_4$ and $CF_4$ are dramatically different from one another. $D_0$ for $CH_4$ decreases

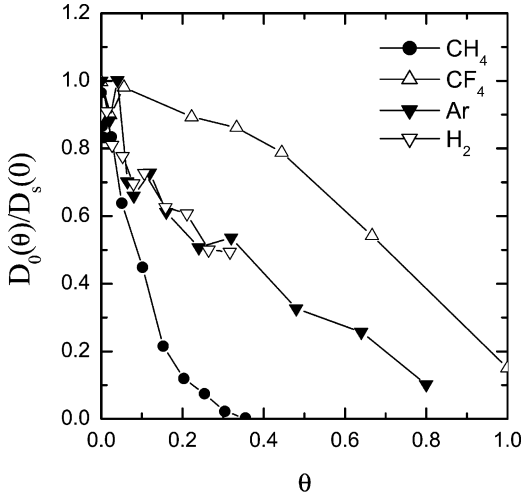


**Figure 11.** Same as Figure 8 but for $CH_4$, $CF_4$, Ar, and $H_2$ in ZSM-12.

rapidly as the loading is increased, although not as rapidly as the self-diffusivity (cf. Figure 7). In contrast, the corrected diffusivity of $CF_4$ drops by only ~10% as $\theta$ is raised from 0 to 0.2. Recall that over the same range, the self-diffusivity of $CF_4$ drops by 2 orders of magnitude (cf. Figure 7). At higher loadings, the corrected diffusivity of $CF_4$ continues to decrease, but $D_0/D(0)$ for $CF_4$ is large at all loadings when compared to the same quantity for $CH_4$. Ar and $H_2$ give corrected diffusivities that behave quite similarly to each other and that behave in a manner intermediate between that seen for $CH_4$ and $CF_4$.

The differences that exist between self-diffusivities and corrected diffusivities arise due to adsorbate−adsorbate correlations.[10,38,39] One way to express these differences that is convenient when working with the Maxwell−Stefan formulation is to write[38]

$$\frac{1}{D_s(\theta)} = \frac{1}{D_0(\theta)} + \frac{\theta}{D_{11}(\theta)} \tag{7}$$

This expression can be regarded as a definition of the self-correlation coefficient, $D_{11}$. Recent work by Skoulidas, Sholl, and Krishna examining binary mixtures of $CH_4$ and $CF_4$ in silicalite has suggested that once $D_{11}$ has been determined for a single-component system, it can be a useful starting point for quantitatively predicting the cross-species diffusivities in multicomponent mixtures.[10] From eq 7 it can be seen that if the self-diffusivity and corrected diffusivity at a particular loading are very similar, then $D_{11}$ is very large. We have determined $D_{11}$ for $CH_4$ in all four of the silica zeolites we have examined, and the results of these calculations are shown in Figure 12. An empirical function that has been suggested to relate $D_{11}$ with the loading dependent corrected diffusivity is[10]

$$\frac{D_{11}(\theta)}{D_0(\theta)} = a \exp(-b\theta) \tag{8}$$

where $a$ and $b$ are adjustable parameters. Application of this function to data from several MD and lattice studies of diffusion in silicalite resulted in values of $b$ varying between 0.7 and 1.4.[10] Equation 8 was found to successfully describe our calculated results for $CH_4$ in silicalite and ITQ-7. We excluded some data for small pore loadings in performing these fits because in this regime the uncertainties in the corrected diffusivity are similar in magnitude to $(D_0(\theta) - D_s(\theta))$. The results of these fits are shown as solid curves in Figure 12 and the associated values

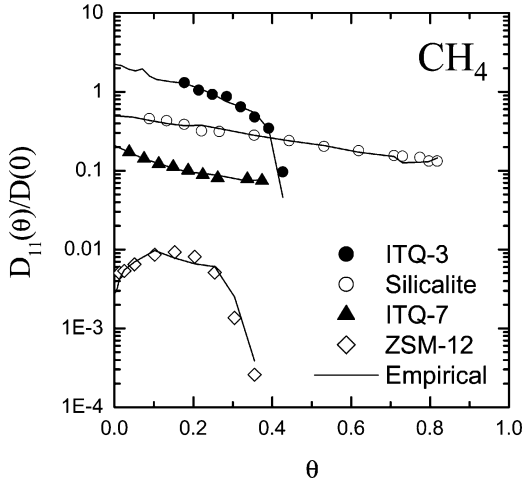


**Figure 12.** $D_{11}(\theta)/D(0)$for $CH_4$ in silicalite, ITQ-3, ITQ-7, and ZSM-12. The data points were determined from EMD simulations, and the solid curves are the fits described in the text.

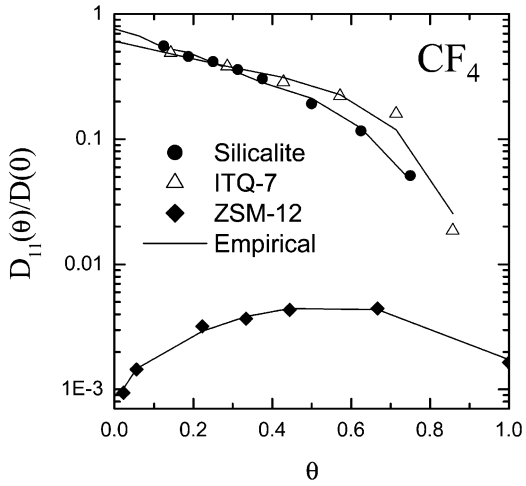


**Figure 13.** Same as Figure 12 but for $CF_4$ in silicalite, ITQ-7, and ZSM-12.

**TABLE 5: Parameters Used in the Fitting Eqs 8 and 9 to the Loading Dependence of $D_{11}$[a]**

| zeolite | species | *a* | *b* | *c* | *d* |
|---|---|---|---|---|---|
| silicalite | $CH_4$ | 0.5 | 1.45 | | |
| | $CF_4$ | 0.736 | 1.30 | | |
| ITQ-7 | $CH_4$ | 0.0245 | −5.70 | 0.190 | 7.3 |
| | $CF_4$ | 0.592 | 1.30 | | |
| ZSM-12 | $CH_4$ | 0.127 | −4.01 | −0.124 | −3.06 |
| | $CF_4$ | 0.738 | −0.0923 | −0.737 | −0.0789 |
| ITQ-3 | $CH_4$ | 2.36 | 7 | | |

[a] All parameters in this table are dimensionless.

of $a$ and $b$ are given in Table 5. The value of $b$ determined for ITQ-3 is strikingly different from the value for silicalite. Equation 8 was not adequate for fitting our data from $CH_4$ diffusion in ITQ-7 or ZSM-12, so we generalized this expression to

$$\frac{D_{11}(\theta)}{D_0(\theta)} = a \exp(-b\theta) + c \exp(-d\theta) \tag{9}$$

The best fits to our data using this expression are shown in Figure 12 as solid curves.

Figure 13 summarizes our results for $D_{11}$ for $CF_4$ in the three zeolites into which this molecule can adsorb. The parameters associated with eqs 8 and 9 are listed in Table 5. The observed

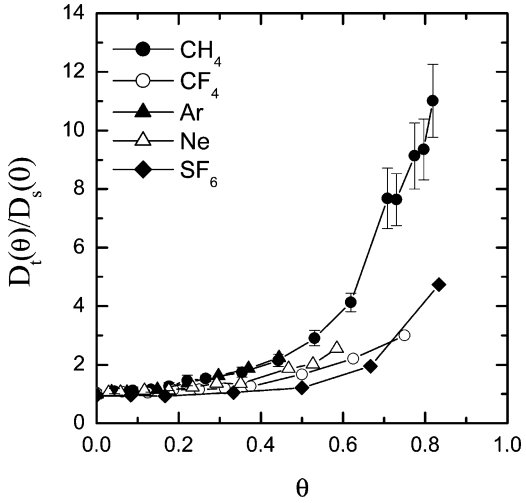


**Figure 14.** $D_t(\theta)/D(0)$ plotted versus $\theta$ for $CH_4$, $CF_4$, $SF_6$, Ar, and Ne in silicalite at 298 K using saturation loadings defined in Table 2.

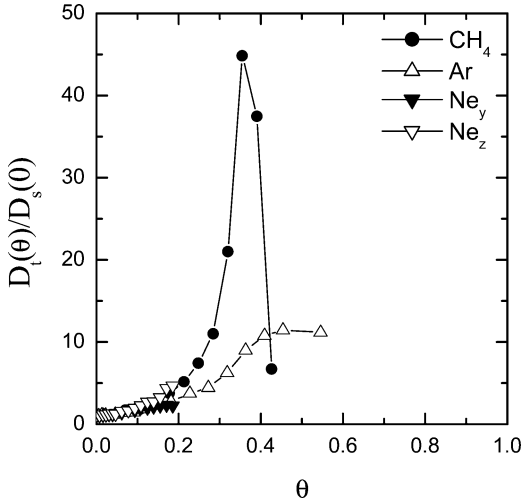


**Figure 15.** Same as Figure 14 but for $CH_4$, Ar, and Ne in ITQ-3.

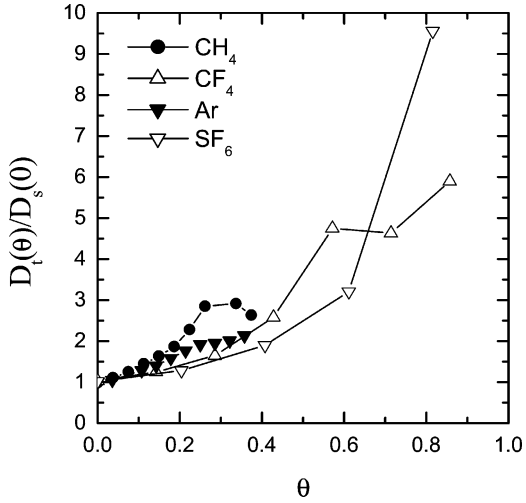


**Figure 16.** Same as Figure 14 but for $CH_4$, $CF_4$, Ar, and $SF_6$ in ITQ-7.

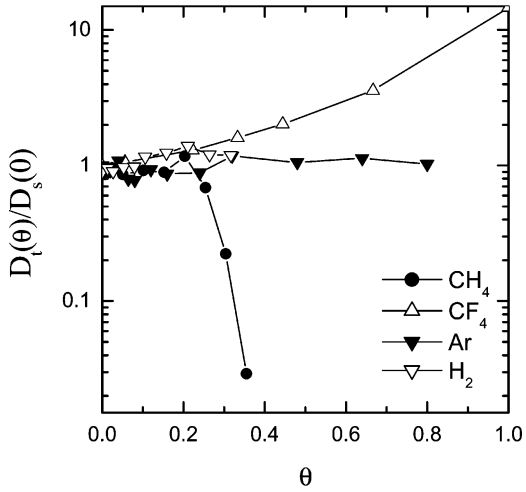


**Figure 17.** Same as Figure 14 but for $CH_4$, $CF_4$, Ar, and $H_2$ in ZSM-12.

behavior of $CF_4$ in silicalite and ITQ-7 is very similar to the results found for $CH_4$ in silicalite. As for $CH_4$, the differences between the self-diffusivities and corrected diffusivities are most dramatic in ZSM-12, so $D_{11}$ for $CF_4$ in ZSM-12 is significantly different than the values seen in the other two materials. The data in Figures 12 and 13 may be useful for making predictions regarding the diffusion properties of $CH_4/CF_4$ mixtures in ITQ-7 and ZSM-12 and comparing these properties to the known properties of this mixture in silicalite.[10,17]

## VI. Transport Diffusion

Though the corrected diffusivity plays a central role in the Maxwell−Stefan formulation of mass transfer, the transport diffusivity plays a central role in Fickian formulations of these processes. As described above, we can compute the transport diffusivity, $D_t$, by determining the corrected diffusivity, $D_0$, from EMD simulations and evaluating the thermodynamic correction factor in eq 3 separately. In the results below, the thermodynamic correction factors have been evaluated from the isotherms given by eq 6. The resulting transport diffusivities, normalized by the infinite dilution diffusivity of each species, are shown in Figures 14−17.

The transport diffusivities observed in silicalite (Figure 14) and ITQ-7 (Figure 16) are qualitatively similar. For each species in these materials, the transport diffusivity is a monotonically increasing function of the pore loading. The transport diffusivities also increase with loading in ITQ-3 (Figure 15), with the exception of the highest loadings examined for $CH_4$, where the transport diffusivity decreases sharply due to rapid decrease in the corrected diffusivity at these loadings (cf. Figure 9).

The transport diffusivities observed in ZSM-12 (Figure 17) exhibit a large range of behaviors. The diffusivities observed for Ar and $H_2$ are almost independent of loading. $CH_4$ has a transport diffusivity that is approximately constant for $\theta \leq 0.3$ but then rapidly decreases by over an order of magnitude at slightly higher loadings. In contrast, the transport diffusivity of $CF_4$ increases strongly with increased loading over the entire range of possible pore loadings.

## VII. Discussion

We have used EMD simulations to describe the single component diffusion of multiple light gases in four different silica zeolites, silicalite, ITQ-3, ITQ-7, and ZSM-12 at room temperature. In each case, we have determined the loading dependent self-diffusivity, corrected diffusivity, and transport diffusivity. Appropriate use of EMD simulations allows these three diffusivities to be determined simultaneously. Although self-diffusion in zeolites has been extensively studied in previous EMD simulations, only a handful of studies have been performed previously that examine corrected and transport diffu-

sivities. The results presented here greatly extend the number and type of examples for which detailed data for the corrected and transport diffusivities are available from atomically detailed simulations.

The general trends observed for the loading dependence of self-diffusion are in good agreement with those found in many previous studies.[2] In silicalite and ITQ-7, whose pores can be described as interconnected pores, self-diffusivities decrease monotonically with loading due to steric hindrance. This effect is more dramatic in the one-dimensional pores of ZSM-12. Self-diffusion in the cage structure of ITQ-3 is controlled by activated cage-to-cage hopping, and adsorbate−adsorbate interactions appear to lower this barrier at low and moderate loadings. Similar effects have been reported previously for light gases diffusing in ZK4, a zeolite with a similar structure.[36,37] For ITQ-3, these effects result in self-diffusivities that increase with pore loadings at low loadings.

Our observations for the corrected diffusivities underline the fact that quantitatively predicting the loading dependence of these quantities remains difficult. The corrected diffusivity is equivalent to the Maxwell−Stefan diffusivity for single component systems. Our earlier EMD simulations of light gases in silicalite[6,13] showed that the so-called Darken approximation, which identifies the corrected diffusivity as a constant independent of loading, is reasonably accurate for some examples, notably $CH_4$, but quite inaccurate for other species such as $CF_4$. A somewhat more refined approximation is to posit that smaller species that are "weakly" confined in the zeolite pores roughly follow the Darken approximation whereas large species that are "strongly" confined show a corrected diffusivity that decreases linearly with fractional loading.[10] The latter behavior is the usual result in lattice models of adsorbate diffusion.[13] This combination of approximation seems adequate to describe the observed range of behaviors in silicalite. Examining the results we have presented here, however, shows that this classification of adsorbed species into smaller and larger species fails to account for the actual behaviors in materials other than silicalite. ITQ-7 is perhaps the most striking example. This material has roughly the same pore topology and diameters as silicalite, but our results show that the largest adsorbates we examined, $SF_6$ and $CF_4$, have the weakest variation in the corrected diffusivity with loading. The smaller adsorbates we studied in ITQ-7, $CH_4$, and Ar, have corrected diffusivities that decrease strongly with loading. In the one-dimensional pores of ZSM-12, the smallest adsorbates, $H_2$ and Ar show a behavior reminiscent of the "strongly" confined species in silicalite, and $CH_4$ has a corrected diffusivity that decreases extremely rapidly as the loading is increased. The corrected diffusivity of the largest species examined in ZSM-12, $CF_4$, exhibits a weaker dependence on loading than any of the other three species. Like the self-diffusivities, the corrected diffusivities observed in ITQ-3 are nonmonotonic functions of pore loading.

The transport diffusivity and corrected diffusivity for an adsorbed component in a zeolite are related by eq 3. All of the systems we have presented here have adsorption isotherms that are well described by the dual Langmuir form, eq 6. As a result, the thermodynamic correction factor in eq 3 is rather similar for all of the systems we have examined. The discussion of the corrected diffusivities above also covers the main points that arise when examining the transport diffusivities.

The results presented here suggest several directions for future work. Though EMD methods can clearly be used to compute how corrected diffusivities vary with loading in zeolites and other microporous materials, it would be useful to develop approximate criteria that predict the trends that will arise from such simulations (or, of course, equivalent experiments). The diversity of the results we report here will place strong requirements on any proposed approximation to resolve this issue. A related issue is the development of approximate methods for predicting mixture transport properties from single-component data. This task can be effectively accomplished for adsorption by using ideal adsorbed solution theory (IAST),[40] but methods that achieve for transport properties the accuracy possible with IAST for adsorption are much less well developed.[10,41] Because the EMD methods used here for single-component systems can also be applied to binary mixtures,[10,15−17] these methods should prove valuable to the future development of approximate models for mixture transport.

Finally, we note that although the EMD simulations used here represent zeolites with fully atomic detail, only noncationic (i.e., all silica) zeolites have been studied here. It is well-known that the presence of framework substitution and accompanying cations in zeolites can have a strong impact on adsorption and diffusion properties in these materials.[42−44] Numerous studies have examined adsorbate self-diffusion in cationic zeolites.[2] Given the availability of suitable interatomic interaction potentials, the EMD methods used here to determine corrected and transport diffusivities can certainly be extended to cationic materials. It seems likely that taking this step would provide useful insight into molecular diffusion in these materials.

**Acknowledgment.** This work was supported by a NSF CAREER award (CTS-9983647). D.S.S. is an Alfred P. Sloan fellow and a Camille Dreyfus Teacher-Scholar.

## References and Notes

(1) Kärger, J.; Ruthven, D. *Diffusion in Zeolites and Other Microporous Materials*; John Wiley & Sons: New York, 1992.
(2) Keil, F. J.; Krishna, R.; Coppens, M. O. *Rev. Chem. Eng.* **2000**, *16*, 71.
(3) Auerbach, S. M. *Int. Rev. Phys. Chem.* **2000**, *19*, 155.
(4) Bowen, T. C.; Falconer, J. L.; Skoulidas, A. I.; Sholl, D. D. *Ind. Eng. Chem. Res.* **2002**, *41*, 1641.
(5) Lai, Z.; Bonilla, G.; Diaz, I.; Nery, J. G.; Sujaoti, K.; Amat, M. A.; Kokkoli, E.; Terasaki, O.; Thompson, R. W.; Tsapatsis, M.; Vlachos, D. G. *Science* **2003**, *300*, 456.
(6) Skoulidas, A. I.; Sholl, D. S. *J. Phys. Chem. B* **2001**, *105*, 3151.
(7) Theodorou, D. N.; Snurr, R. Q.; Bell, A. T. Molecular Dynamics and diffusion in microporous materials. In *Comprehensive Supramolecular Chemistry*; Alberti, G., Bein, T., Eds.; Pergamon Press: New York, 1996; Vol. 7; p 507.
(8) Krishna, R.; Vandenbroeke, L. J. P. *Chem. Eng. J. Bioch. Eng.* **1995**, *57*, 155.
(9) Paschek, D.; Krishna, R. *Langmuir* **2001**, *17*, 247.
(10) Skoulidas, A. I.; Sholl, D. S.; Krishna, R. *Langmuir* **2003**, *19*, 7977.
(11) Jobic, H. *Curr, Opin, Solid State Mater. Sci.* **2003**, *6*, 415.
(12) Reyes, S. C.; Sinfelt, J. H.; DeMartin, G. J. *J. Phys. Chem. B* **2000**, *104*, 5750.
(13) Skoulidas, A. I.; Sholl, D. S. *J. Phys. Chem. B* **2002**, *206*, 5058.
(14) Jobic, H.; Karger, J.; Bee, M. *Phys. Rev. Lett.* **1999**, *82*, 4260.
(15) Sanborn, M. J.; Snurr, R. Q. *Sep. Purif. Technol.* **2000**, *20*, 1.
(16) Sanborn, M. J.; Snurr, R. Q. *AIChE J.* **2001**, *47*, 2032.
(17) Skoulidas, A. I.; Bowen, T. C.; Doelling, C. M.; Falconer, J. L.; Noble, R. D.; Sholl, D. S. *J. Membr. Sci.*, in press.
(18) Fyfe, C. A.; Gies, H.; Kokotailo, G. T.; Marler, B.; Cox, D. E. *J. Phys. Chem.* **1990**, *94*, 3718.
(19) Camblor, M. A.; Corma, A.; Lightfoot, P.; Villaescusa, L. A.; Wright, P. A. *Angew. Chem., Int. Ed. Engl.* **1997**, *36*, 2959.
(20) Villaescusa, L. A.; Barret, P. A.; Camblor, M. A. *Angew. Chem., Int. Ed.* **1999**, *38*, 1997.
(21) Olson, D. H.; Kokotailo, G. T.; Lawton, S. L.; Meier, W. M. *J. Phys. Chem.* **1981**, *85*, 2238.
(22) Skoulidas, A. I.; Ackerman, D. M.; Johnson, J. K.; Sholl, D. S. *Phys. Rev. Lett.* **2002**, *89*, 185901.
(23) Kärger, J.; Petzold, M.; Pfeifer, H.; Ernst, S.; Weitkamp, J. *J. Catal.* **1992**, *136*, 283.
(24) Lei, G. D.; Carvill, B. T.; Sachtler, W. M. H. *Appl. Catal. A: Gen.* **1996**, *142*, 347.

(25) Hahn, K.; Karger, J.; Kukla, V. *Phys. Rev. Lett.* **1996**, *76*, 2762.
(26) Keffer, D.; McCormick, A. V.; Davis, H. T. *Mol. Phys.* **1996**, *87*, 367.
(27) Sholl, D. S.; Fichthorn, K. A. *J. Chem. Phys.* **1997**, *107*, 4384.
(28) Sholl, D. S.; Fichthorn, K. A. *Phys. Rev. Lett.* **1997**, *79*, 3569.
(29) Sholl, D. S. *Chem. Eng. J. Bioch. Eng.* **1999**, *74*, 25.
(30) Hahn, K.; Kärger, J. *J. Phys. Chem. B* **1998**, *102*, 5766.
(31) Sholl, D. S. *Ind. Eng. Chem. Res.* **2000**, *39*, 3737.
(32) Fuchs, A. H.; Cheetham, A. K. *J. Phys. Chem. B* **2001**, *105*, 7375.
(33) Doulsin, D. R.; Harrison, R. H.; Moore, R. T. *J. Phys. Chem.* **1967**, *71*, 3477.
(34) Dymond, J. H.; Smith, E. B. *The Virial Coefficients of Gases − A Critical Compilation*; Clarendon Press: Oxford, U.K., 1969.
(35) Goj, A.; Sholl, D. S.; Akten, E. D.; Kohen, D. *J. Phys. Chem. B* **2002**, *106*, 8367.
(36) Tunca, C.; Ford, D. M. *J. Chem. Phys.* **1999**, *111*, 2751.
(37) Tunca, C.; Ford, D. M. *J. Phys. Chem. B* **2002**, *106*, 10982.
(38) Krishna, R.; Paschek, D. *Phys. Chem. Chem. Phys.* **2002**, *4*, 1891.
(39) Kärger, J.; Vasenkov, S.; Auerbach, S. M. Diffusion in Zeolites. Chapter 10. In *Handbook of Zeolite Science and Technology*; Auerbach, S. M., Carrado, K. A., Dutta, P. K., Eds.; Marcel Dekker: New York, 2003.
(40) Smit, B.; Krishna, R. *Chem. Eng. Sci.* **2003**, *58*, 557.
(41) Krishna, R. *Chem. Phys. Lett.* **2002**, *355*, 483.
(42) Coppens, M. O.; Bell, A. T.; Chakraborty, A. K. *Chem. Eng. Sci.* **1999**, *54*, 3455.
(43) Chen, L. G.; Falcioni, M.; Deem, M. W. *J. Phys. Chem. B* **2000**, *104*, 6033.
(44) Beerdsen, E.; Smit, B.; Calero, S. *J. Phys. Chem. B* **2002**, *106*, 10659.
(45) Goodbody, S. J.; Watanabe, K.; MacGowan, D.; Quirke, N. *J. Chem. Soc., Faraday Trans.* **1991**, *87*, 1951.
(46) Heuchel, M.; Snurr, R. Q.; Buss, E. *Langmuir* **1997**, *13*, 6795.
(47) Clark, L. A.; Gupta, A.; Snurr, R. Q. *J. Phys. Chem. B* **1998**, *102*, 6720.